

# Quantifying stimulus-induced periodic modulation in non-Poisson spike trains

Daniel A. Wagenaar, Matthew H. Rosenberg, and Markus Meister

Technical Report November 10, 2021

## 1 Introduction

We are engaged in a large-scale collaboration to find evidence of magnetoreception in the nervous systems of multiple species. Each lab in the collaboration presents periodic magnetic stimuli while recording from whichever area of the nervous system they study in the course of their other projects. The stimulus in all cases consists of a magnetic field that oscillates, typically at a few Hz, with a strength comparable to or larger than the earth magnetic field. The lab then processes the raw data by their own standard methods, and shares the resulting recordings with the collaboration.

Here we focus on the case where the recordings are spike trains. The central question becomes: Do those spike trains exhibit any modulation induced by the stimulus? Detecting modulation in continuous time series is a well-explored subject. Detecting modulation in a point process (such as a spike train) is somewhat less common. Here, we will describe one method that can detect stimulus-induced modulations, and also yields an upper bound on the magnitude of modulations that would remain undetected. When applied to 5 data sets of recordings from zebra finch brain, the method revealed no significant modulations of firing rate at the magnetic field frequency.

## 2 The data

We analyzed spike trains recorded with silicon probes from a 1.3 year old female zebra finch. The experimental pipeline comprised three phases: surgical preparation, acclimation to restraint, and awake electrophysiology. All procedures followed animal welfare guidelines under a protocol reviewed and approved by the Caltech IACUC.

### 2.1 Craniotomies and headpost implantation for neural recordings

The animal was anesthetized with isoflurane, a small head post was cemented to the skull (C&B metabond), and two small craniotomies were opened—one for insertion of the electrode anterior to the midsagittal bifurcation and another over the cerebellum for the ground/reference wire ( $\sim 1\text{-}2.5$  and 1 mm diameter respectively). The craniotomies and exposed skull were then covered with bio-compatible polymer (Kwik-sil). All surgical procedures were conducted under sterile conditions and with standard postoperative pain management.

## **2.2 Acclimation to restraint**

The animal was acclimated to restraint and head fixation 5–14 days after the surgical procedure. The animal experienced three sessions of increasing duration (30 minutes, 1 hour, and 2 hours) spread across three days. On each day, the animal was restrained in a plastic (Falcon) tube to prevent injury to the animal or probe damage during the recording session resulting from wing flapping. The head was immobilized by clamping the headpost to a fixed arm.

## **2.3 Awake electrophysiology**

Neural recordings were collected from a Neuropixels probe system (Janelia, version 3B1) with a National Instruments USB-6221 DAQ and SpikeGLX software.

Prior to the recording session, the probe was coated with Dil to facilitate reconstruction of the probe path in subsequent histology. The animal was restrained in the plastic tube and head-fixed as during the acclimation phase. The craniotomies were exposed, the ground/reference wire was implanted in the cerebellum and secured with Kwik-sil, and the probe was inserted with a micromanipulator. A drop of mineral oil was placed over the insertion site to keep it moist during the recording. After waiting for the signals to settle, experimental recordings began. Each recording had a duration of approximately 5 minutes in which different types of stimuli were presented to the bird.

A magnetic field was generated using custom solenoids (see "MagnetSearch Collaboration Plan" for specifications) driven by a function generator with sinusoidal voltage at 3 Hz or 5 Hz frequency. Two solenoids were placed on either side of the animal under the beak with the axis oriented toward the head, approximately 45 degrees down from the sagittal plane. The magnetic field amplitude at the location of the bird head exceeded the strength of the Earth's magnetic field.

Seven recordings were collected under continuous sinusoidal magnetic stimulation. One of these was excluded due to an artifact in the magnetic stimulus; another was excluded due to excessive noise across all channels. Two of the five recordings were conducted with 3 Hz stimulation, the other three with 5 Hz stimulation. Seven additional recordings were collected but not analyzed here (steady-state, settling, and metronome stimulus).

## **2.4 Spike sorting**

Raw recordings from the Neuropixels probes were referenced to the average across all electrodes. Spike sorting was performed with Kilosort2. Units with excessive noise or abnormal spike waveforms were excluded. Ambiguous cases were included in the analysis to diminish the chances of excluding magneto-sensitive cells during spike sorting.

## 3 Mathematical basics

### 3.1 Fourier series

Any (reasonable) real- or complex-valued function  $g(t)$  defined on the finite interval  $[0, T]$  can be written as a linear superposition of complex exponentials:

$$g(t) = \sum_{n=-\infty}^{+\infty} e^{2\pi i n t / T} c_n.$$

Here  $e^{2\pi i n t / T}$  is the complex exponential with frequency  $f = n/T$ ,  $c_n$  denotes the weight of the contribution from that exponential, and the sum combines contributions from all different frequencies. The numbers  $c_n$  are known as the *Fourier coefficients* of  $g(t)$  and are given by:

$$c_n = \frac{1}{T} \int_0^T e^{-2\pi i n t / T} g(t) dt.$$

### 3.2 Fourier coefficients of a point process

Fourier analysis as described above is usually applied to time series data, i.e., data that are described by a function of (continuous or discretized) time. However, the same basic analysis can be applied to point processes, i.e., data that consist of a sequence of timestamps, such as spike trains. That is because a spike train comprising  $N$  spikes at times  $t_k$  (where  $k = 1 \dots N$ ) can be written as a function:

$$g(t) = \sum_{k=1}^N \delta(t - t_k),$$

where  $\delta(x)$  is the Dirac delta function (whose value is zero every except at  $x = 0$  and whose integral is one). Thus, the Fourier coefficients of a spike train  $\{t_k\}$  are:

$$c_n = \frac{1}{T} \sum_k e^{-2\pi i n t_k / T}. \quad (1)$$

To gain an intuition of what this means, consider two alternative spike trains comprising 10 spikes in a 10-s recording period: In the first train spikes happen at perfectly regular intervals (Fig. 1A); in the second they occur at irregular intervals (Fig. 1B). When analyzed at the frequency of the spikes, the former will yield a large (absolute) value for  $c_n$ , because the phasors  $e^{-2\pi i n t_k / T}$  align constructively, producing a large sum in the complex plane. The latter yields a much smaller value for  $c_n$ , since the phasor  $e^{-2\pi i n t_k / T}$  will be different for each of the spikes, so the vector sum is smaller. Finally, if a periodic spike train is analyzed at a frequency other than the firing rate (or its multiples), the phasors sum destructively and the resulting Fourier coefficient is close to zero (Fig. 1C).

## 4 Detecting modulation in spike trains

For simplicity we choose our recording interval  $T$  such that it is an exact multiple of the period of the stimulus, i.e., such that  $f_s T$  is integer, where  $f_s$  is the frequency of the stimulus. In that

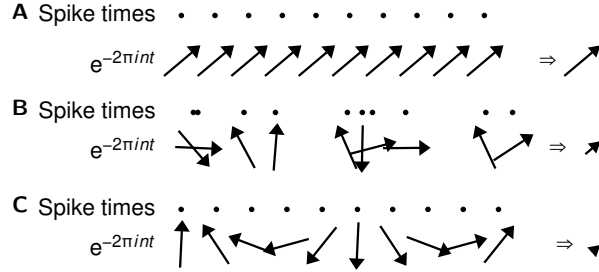


**Figure 1:** Fourier analysis of point processes. **A.** Fourier analysis of a periodic spike train at the frequency of that spike train. Arrows represent the complex exponential (phasor) connected to each spike time. All the phasors are aligned and produce a large sum vector. **B.** Fourier analysis of a train of irregularly timed spikes. Here the phasors point in random directions. **C.** Fourier analysis of a periodic spike train at a different frequency. Here the phasors are systematically arranged at different phases, and thus cancel destructively.

scenario, the Fourier coefficient at the frequency of the stimulus is  $c_s := c_{n=f_s T}$ . If this coefficient is significantly elevated in the presence of a stimulus, one may conclude that the spike train is modulated by that stimulus.

The obvious question is: What constitutes significant elevation? It helps to consider some toy models for the statistics of the spike train and evaluate the predicted Fourier coefficients.

#### 4.1 Warm-up exercise: assuming Poisson statistics

If the spike train is a homogeneous Poisson process, then spikes happen independently of each other and with constant probability per unit time. This implies that the phasors  $e^{-2\pi i n t_k / T}$  (Fig. 1B) have uniformly distributed random phases in the complex plane. Thus the Fourier coefficient  $c_n$  of Eqn. 1 is  $1/T$  times the sum of  $N$  random unit arrows in the complex plane, whose phase angles are independently and uniformly distributed. This is true at all frequencies  $n$ , so we will drop the index on  $c$  for notational convenience:

$$c = \frac{1}{T} \sum_{k=1}^N s_k, \quad (2)$$

where  $s_k$  is a random phasor

$$s_k = e^{-2\pi i \phi_k},$$

with  $\phi_k$  uniformly distributed in  $[0, 2\pi]$ . One can show that the absolute value  $|c|$  is distributed as

$$P(|c|) = \frac{2|c|T}{R} e^{-|c|^2 T/R}, \quad (3)$$

where  $R = N/T$  is the firing rate of the Poisson process. (See the Appendix for a derivation of this result.)

Of course one can easily simulate the Poisson process numerically. For Figure 2 we simulated 10,000 examples of spike trains, each spanning 100 s at a given firing rate. We show the distribution of all Fourier amplitudes from these spike trains. As can be seen, it nicely matches the analytical result. This probability distribution represents a prediction from the null hypothesis that the spike train is Poisson at constant rate with no modulation from the

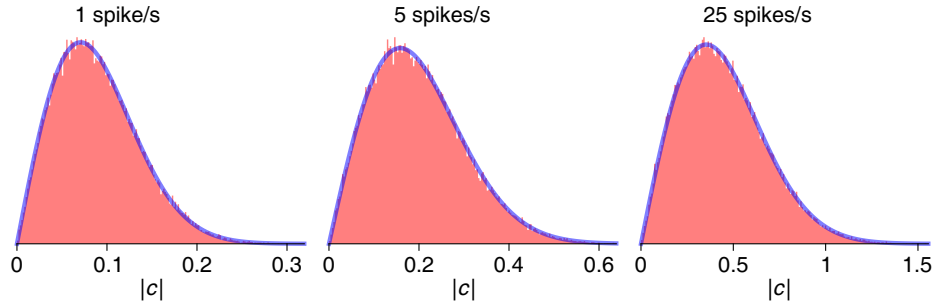


**Figure 2:** Fourier coefficients from artificial spike trains that obey Poisson statistics. Constructed from 10,000 instances of 100-s long artificial “recordings.” Pink: sampled distribution. Blue: prediction from Eqn 3.

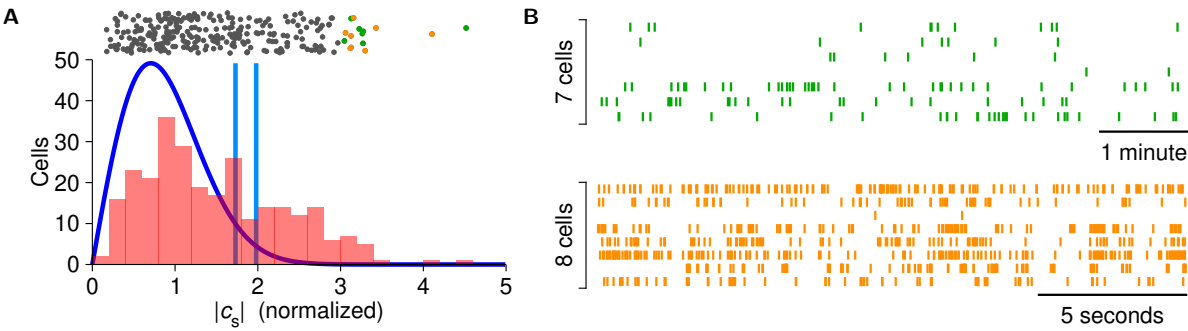


**Figure 3:** False positive detections resulting from incorrect assumption of Poisson statistics. **A.** Histogram of Fourier coefficients at  $f = 4$  Hz for 275 cells recorded for 400 s in the absence of a stimulus at the analysis frequency (*pink*) with theoretical curve assuming Poisson statistics (*blue*). The 95th and 98th percentiles of the theoretical distribution are indicated by light blue lines. Many of the measured coefficients lie beyond the 98th percentile under the Poisson assumption and would be flagged as positive results. *Dots*: Data for individual cells. Colored dots correspond to examples in **B**. **B.** Spike trains from cells with the highest Fourier coefficients: 7 cells with relatively low firing rates (*top*) and 8 cells with relatively high firing rates (*bottom*). Note the pronounced temporal clusters of spikes.

magnetic field or anything else. For an experimental spike train, one can now compare the measured Fourier coefficients to this probability distribution and derive a likelihood for the null model.

## 4.2 The Fourier components of actual spike trains

Unfortunately, real spike trains rarely obey Poisson statistics. One well-known deviation is the refractory period, a brief obligatory silent interval following each spike. Many spike trains are also “bursty”, in the sense that spikes tend to come in clusters that are separated by longer intervals. So spikes “repel each other” at short intervals of 1–2 ms but often attract each other at longer intervals. Both are obvious discrepancies from the Poisson model of independent spikes. As a result, a comparison to predictions from Poisson behavior leads to large numbers of false positive detections of modulation (Fig. 3).

Our task here is well-defined: to detect modulation at one specific frequency, namely that of the oscillating magnetic field. Figure 4 suggests a simple approach: Within some range of

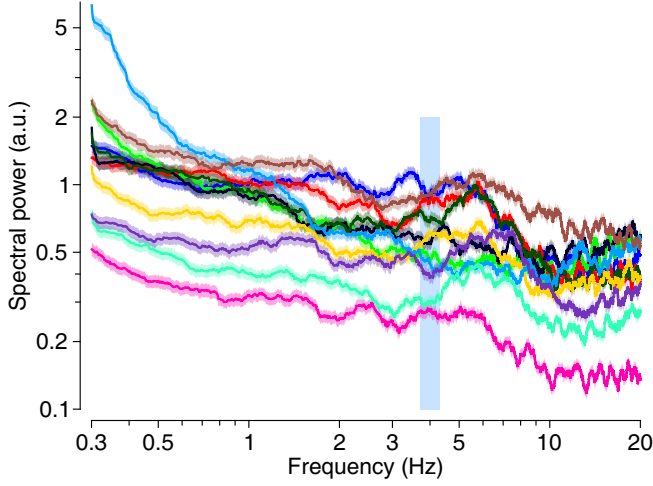


**Figure 4:** Multitaper power spectra of several spike trains.

the modulation frequency (say  $4.0 \pm 0.3$  Hz) the power spectra look reasonably flat. It appears that the Fourier coefficients in this range are drawn from approximately the same distribution. So we can compare the Fourier coefficient at the stimulus frequency with a probability distribution constructed from all the other coefficients in that limited range.

Figure 5 illustrates the results. For a given spike train, the Fourier coefficients within the range of interest ( $4.0 \pm 0.3$  Hz) scatter with a distribution that appears independent of frequency (Fig. 5A) and that follows a Gaussian shape (Fig. 5B). Comparing across cells, the variance of that distribution increases with the firing rate (Fig. 5C), as expected because more phasors contribute to the coefficient (Fig. 1). However the mean of the distribution, the skewness, and the kurtosis all remain near zero (Fig. 5D–F). All this suggests that the Fourier coefficients follow a Gaussian distribution to good approximation.

These observations can be used for a revised test of the null hypothesis: If there is no modulation by the stimulus, then the Fourier coefficient at the stimulus frequency,  $c_s$ , should be drawn from the same Gaussian distribution as the coefficients at nearby frequencies  $c_{n \neq f_s T}$ . For a useful statistic we define the *normalized response* as the absolute value of the Fourier coefficient at the stimulus frequency normalized by the standard deviation of the Fourier coefficients at non-stimulus frequencies:

$$\hat{c} = \frac{|c_s|}{\sigma_c}. \quad (4)$$

where

$$\sigma_c = \sqrt{\langle |c_n|^2 \rangle_{n \neq f_s T}} \quad (5)$$

Under the null hypothesis,  $c_s$  should be distributed just like the other  $c_n$ , which implies that  $\hat{c}$  should be distributed as

$$P(\hat{c}) = \hat{c} e^{-\frac{1}{2}\hat{c}^2} \quad (6)$$

(see Appendix). The actually observed values of  $\hat{c}$  can then be compared against this null model, and much as in Figure 3, we can test whether any neurons produce unexpectedly large values of  $\hat{c}$ . Figure 6 shows that this is not the case. About 5% of the neurons fall above the 95th percentile of the null distribution, and no unusually large values occur. In other words these data appear consistent with the null hypothesis of “no modulation”.

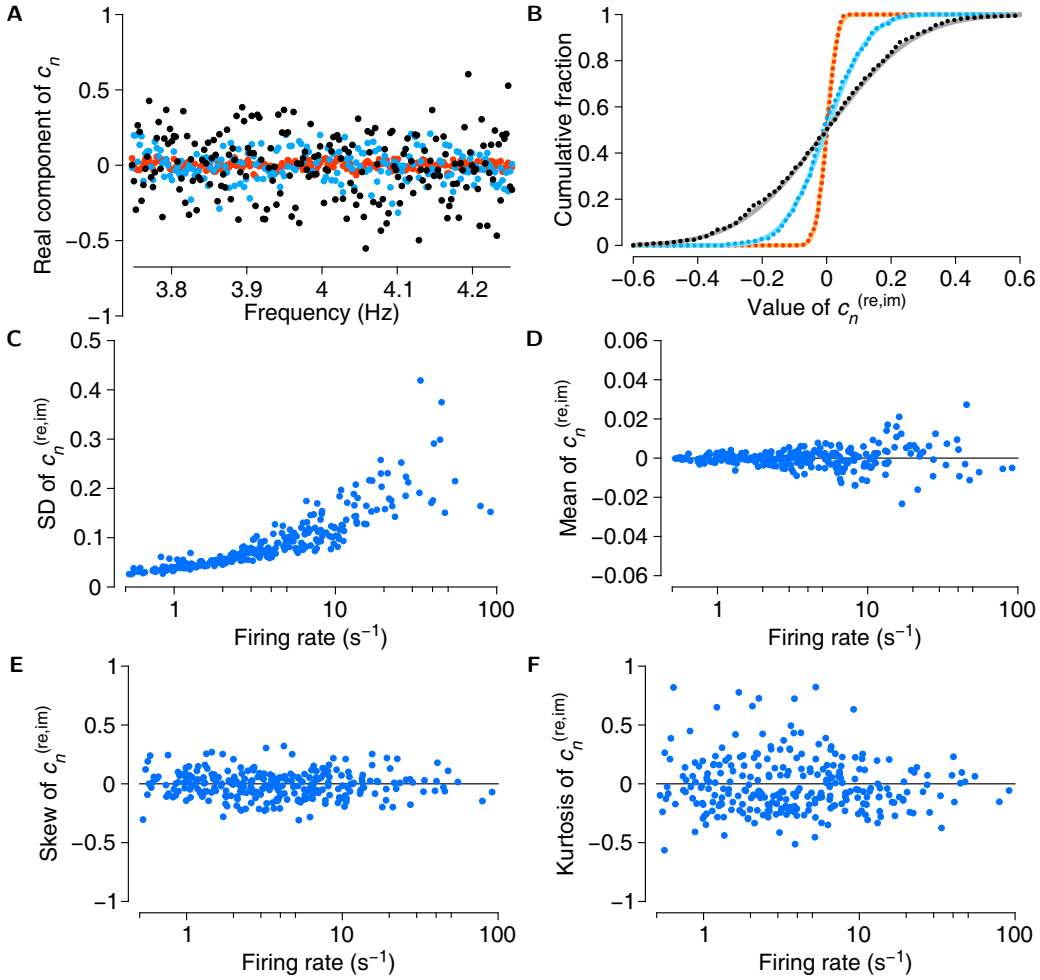


**Figure 5:** **A.** Real components of the Fourier coefficients as a function of frequency from three actual spike trains, with firing rates of  $0.5\text{ s}^{-1}$  (red),  $10\text{ s}^{-1}$  (blue), and  $55\text{ s}^{-1}$  (black). Recording time: 400 s. **B.** Cumulative distribution of the data shown in A (dotted lines) compared with best-fit zero-mean Gaussian. **C.** Standard deviation of Fourier components for each of 275 recorded cells plotted against their firing rates. **D–F.** Means, skew, and kurtosis of Fourier components, ditto.

### 4.3 Confidence limits on modulation

Hypothesis testing for the presence of modulation is not the only use for the null model described in the previous section. The model can also be used to generate confidence limits on undetected modulation.

To explore this, we start from actually recorded spike trains  $\{t_k\}$  that have no stimulus-induced modulation, and introduce artificial modulation at a defined frequency  $f_s$ . This is done by shifting some of the spikes by half a stimulus period. The probability that a spike at time  $t_k$  will get shifted varies sinusoidally in time

$$p(t_k) = \frac{A}{2} [1 + \cos(2\pi f_s t_k)],$$

where  $A$  represents modulation amplitude and  $f_s$  is the frequency of the modulation. The resulting spike train has the same mean firing rate, but its rate is modulated at the frequency  $f_s$  with relative amplitude (peak/mean – 1) given by  $A$ .

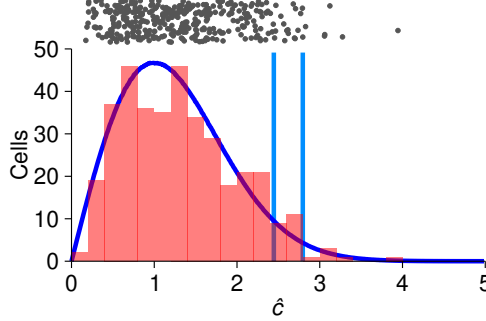


**Figure 6:** A test for modulation using the improved null model: Histogram (*pink*) of the normalized responses  $\hat{c}$  from all neurons (*dots*) along with the predicted null distribution (*blue*). Vertical lines indicate 95th and 98th percentiles of the null distribution.

We took 275 actual spike trains with firing rates ranging between 0.5 and 91 spikes/s, each of 400-s duration, and created artificially modulated copies of each, at modulation amplitudes ranging from  $A = 0.01$  (1%) to 0.5 (50%). For each spike train and modulation amplitude, we calculated 1000 instances of artificially modulated spike trains. For each cell, we compared the actual  $\hat{c}$ -value of the original spike train (Eqn 4) with the 1000 artificial  $\hat{c}$ -values in each group. We found the maximum level of modulation where the actual  $\hat{c}$  would be in the lowest 95% of the distribution, and plotted the result in Figure 7A. These data represent our 95% confidence limits on the modulation in the actual spike trains.

Unsurprisingly, these confidence limits depend rather steeply on the firing rate of the cell. However, we noted that these confidence limits also varied substantially among cells with very similar firing rates. To test whether this was an artifact of our sampling procedure, we grouped the 1000 instances of artificially modulated spike trains into 10 groups of 100 (for each cell and at each modulation level), and repeated the above calculation within each group. The population standard deviation among groups is plotted for each cell as error bars in Figure 7. The fact that these error bars are small compared to the overall spread in the data indicates that differences in detection limits are due to inherent differences in firing statistics between cells rather than to our sampling procedure.

Another way to think about these results is to ask how small a modulation would be detectable with our method in spike trains with statistics like our recordings. To explore this, we again used the artificially modulated spike trains and applied the test of Figure 6 at various confidence levels. We asked what level of modulation would be detected by that method at least 50% of the time, and called that the “minimum detectable modulation” (Fig 7B). We may conclude that a cell with a firing rate of 2 spikes/s would need a modulation of 0.25 to be detectable with confidence  $p < 10^{-4}$ , whereas in a cell firing 50 spikes/s a modulation of only 0.05 would be detectable at the same confidence level. Unsurprisingly, the more relaxed the confidence level, the smaller modulations are detectable, but the effect of going from  $p < 10^{-4}$  (appropriate when analyzing up to 500 spike trains in parallel) to  $p < 0.01$  (appropriate for up to 5 spike trains) is not as large as one might have imagined.

#### 4.4 Results from magnetic stimulation

Having shown that our method produces a null model that accurately describes the observations at frequencies where no stimulus-induced modulation was expected, we now turn to an-

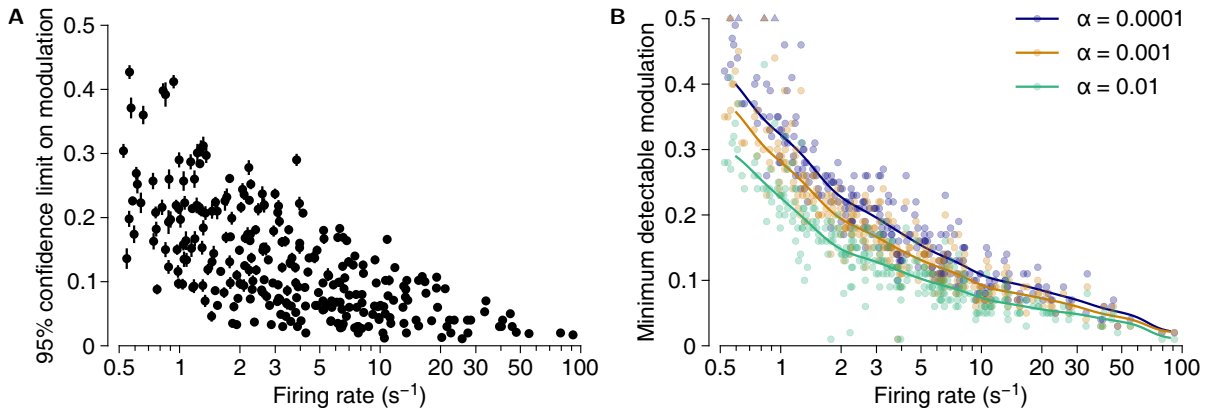


**Figure 7:** Detectability of stimulus-induced modulations. **A.** Confidence limits on the magnitude of periodic modulation. Each dot represents a spike train from a different neuron. The confidence limit is based on comparison with artificially modulated versions of the same spike train. **B.** Minimum detectable modulation for spike trains with different firing rates at several levels  $\alpha$  of false-positive detection. Lines are interpolations of the data. Triangles mark outliers: spike trains for which no level of modulation up to 0.5 yielded detectability.

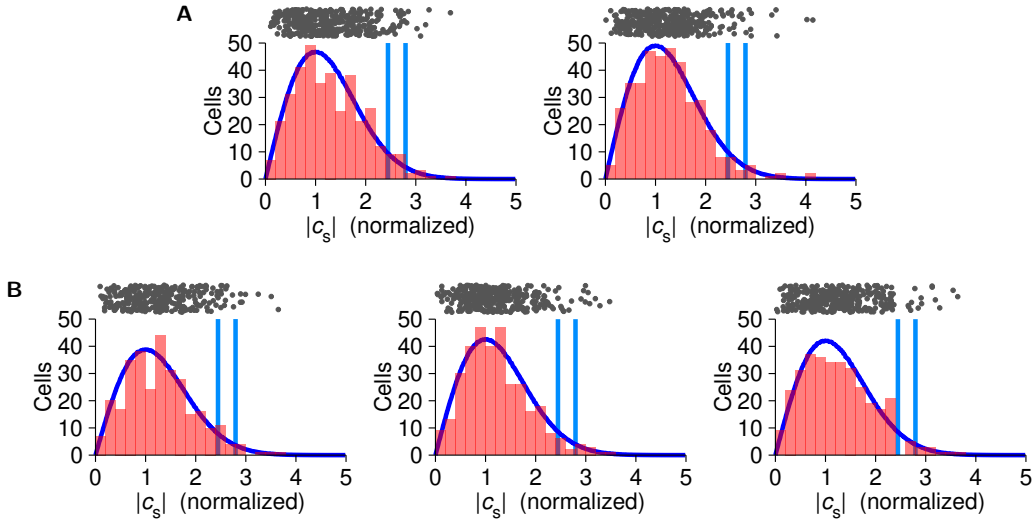


**Figure 8:** Analysis of recordings during magnetic stimulation. Display as in Fig 6. **A.** Two recordings during 3-Hz stimulation. **B.** Three recordings during 5-Hz stimulation.

alyzing the data at the actual stimulus frequency. Using two recordings from animals exposed to magnetic fields oscillating at 3 Hz and three recordings at 5 Hz, we repeated the above procedures, analyzing each recording at its stimulation frequency (Fig. 8). No cells in any of the experiments exhibited modulation exceeding what would be expected from the null model.

# Appendix: Derivations of probability distributions

## A.1 The normal distribution in two dimensions

(This derivation, which can be found in many textbooks, is given here for easy reference and to introduce notation.)

Let  $X$  be a random variable, normally distributed with mean  $\mu = 0$  and variance  $\sigma^2$ . The probability distribution of  $X$  is the well-known bell curve:

$$P(x) = \frac{1}{\sqrt{2\pi\sigma^2}} e^{-\frac{1}{2}x^2/\sigma^2}.$$

Let  $Y$  be a second such random variable, same distribution, independent of  $X$ . Then the joint probability distribution of  $X$  and  $Y$  is

$$P(x, y) = \frac{1}{2\pi\sigma^2} e^{-\frac{1}{2}(x^2+y^2)/\sigma^2}. \quad (7)$$

Let us now introduce  $R = \sqrt{X^2 + Y^2}$ . What is the distribution of  $R$ ? We can find out by transforming to polar coordinates ( $X = R \cos\Theta$ ,  $Y = R \sin\Theta$ ):

$$P(r, \theta) = P(x, y) \left| \frac{\partial x}{\partial r} \frac{\partial y}{\partial \theta} \right| = r P(x, y). \quad (8)$$

Since the distribution (Eqn. 7) is obviously independent of the angle  $\theta$ , we have

$$P(\theta) = \frac{1}{2\pi}$$

and hence

$$P(r, \theta) = P(r)P(\theta) = \frac{1}{2\pi} P(r). \quad (9)$$

Combining Eqns. 7, 8, and 9, we conclude:

$$P(r) = \frac{r}{\sigma^2} e^{-\frac{1}{2}r^2/\sigma^2}. \quad (10)$$

If the variable of interest is normalized to unit standard deviation, such that  $\langle r^2 \rangle = \sigma^2 = 1$  then

$$P(r) = r e^{-\frac{1}{2}r^2} \quad (11)$$

as used in Eqn 6.

## A.2 Fourier coefficients of Poisson spike trains

As shown in Eqn 2, the Fourier coefficients of a Poisson spike train with  $N$  spikes all have the same probability distribution: they are essentially the sum of  $N$  random unit vectors in the 2-dimensional plane. Say

$$\mathbf{u} = \sum_{i=1}^N \mathbf{s}_i,$$

where the  $\mathbf{s}_i$  are random unit vectors. Then the covariance matrix of  $\mathbf{u}$  is

$$\begin{aligned}\mathbf{C} &= \langle \mathbf{u} \mathbf{u}^\top \rangle = \sum_i \langle \mathbf{s}_i \mathbf{s}_i^\top \rangle + \sum_{i \neq j} \langle \mathbf{s}_i \mathbf{s}_j^\top \rangle \\ &= N \langle \mathbf{s} \mathbf{s}^\top \rangle + \sum_{i \neq j} \langle \mathbf{s}_i \rangle \langle \mathbf{s}_j \rangle^\top \\ &= \frac{N}{2} \mathbf{1},\end{aligned}$$

where all the sums are from 1 to  $N$ , and  $\mathbf{1}$  is the identity matrix. To understand the last step note that for a random unit vector in two dimensions

$$\langle \mathbf{s} \mathbf{s}^\top \rangle = \begin{pmatrix} \langle x^2 \rangle & \langle xy \rangle \\ \langle yx \rangle & \langle y^2 \rangle \end{pmatrix}. \quad (12)$$

Because of normalization  $\langle x^2 \rangle + \langle y^2 \rangle = 1$ , and because of symmetry  $\langle x^2 \rangle = \langle y^2 \rangle$  and  $\langle xy \rangle = 0$ . Therefore  $\langle \mathbf{s} \mathbf{s}^\top \rangle = \frac{1}{2} \mathbf{1}$ .

If  $N$  is reasonably large, the Central Limit Theorem applies: Since  $\mathbf{u}$  is the sum of many independent random variables, its distribution is a Gaussian with the same covariance matrix as  $\mathbf{u}$ :

$$\begin{aligned}P(\mathbf{u}) &= \frac{1}{2\pi\sqrt{\det \mathbf{C}}} e^{-\frac{1}{2} \mathbf{u}^\top \mathbf{C}^{-1} \mathbf{u}} \\ &= \frac{1}{\pi N} e^{-\frac{\|\mathbf{u}\|^2}{N}}.\end{aligned}$$

The Fourier coefficient (Eqn. 2) is

$$\mathbf{c} = \frac{1}{T} \mathbf{u},$$

so its distribution is the 2-D Gaussian

$$P(\mathbf{c}) = \frac{T^2}{\pi N} e^{-\frac{T^2 \|\mathbf{c}\|^2}{N}}.$$

Using Eqn 10 one concludes that the vector length of  $\mathbf{c}$  has distribution

$$P(\|\mathbf{c}\|) = \frac{2\|\mathbf{c}\| T^2}{N} e^{-\|\mathbf{c}\|^2 T^2 / N},$$

as used in Eqn 3. (Note that in the main text, we introduced  $c$  as a complex number, whereas here we discussed  $\mathbf{c}$  as a 2D vector. The difference is immaterial, since addition and absolute value ( $|c|$ ) for complex numbers are defined in terms of real and imaginary components just as addition and vector length ( $\|\mathbf{c}\|$ ) are for 2D vectors.)